Received: 10 February 2023 | Revised: 31 May 2023 | Accepted: 23 June 2023

DOI: 10.1002/nbm.5004

RESEARCH ARTICLE

NMR IN BIOMEDICINE WILEY

Vascular differences between *IDH*-wildtype glioblastoma and astrocytoma *IDH*-mutant grade 4 at imaging and transcriptomic levels

María del Mar Álvarez-Torres[1] | Adolfo López-Cerdán[2] | Zoraida Andreu[3] | Maria de la Iglesia Vayá[2] | Elies Fuster-Garcia[1] | Francisco García-García[4] | Juan M. García-Gómez[1]

[1]Biomedical Data Science Laboratory, ITACA (Instituto de Información y Tecnología de las Comunicaciones), Universitat Politècnica de València, Valencia, Spain

[2]Unidad Mixta de Imagen Biomédica FISABIO-CIPF (Centro Investigación Príncipe Felipe), Valencia, Spain

[3]Foundation Valencian Institute of Oncology (FIVO), Valencia, Spain

[4]Unidad de Bioinformática y Bioestadística del CIPF, Valencia, Spain

Correspondence
María del Mar Álvarez-Torres, Biomedical Data Science Laboratory, ITACA (Instituto de Información y Tecnología de las Comunicaciones), Universitat Politècnica de València, Valencia, Spain.
Email: maaltor4@upv.es

Funding information
This study was funded by: Grant PID2019-104978RB-I00/AEI/10.13039/501100011033 (ALBATROSS) funded by MCIN/AEI/ 10.13039/501100011033, Grant PID2021-127110OA-I00 (PROGRESS) funded by MCIN/AEI/10.13039/501100011033 (both from Agencia de Investigación de Espana) and by ERDF A way of making Europe.

Abstract

Global agreement in central nervous system (CNS) tumor classification is essential for predicting patient prognosis and determining the correct course of treatment, as well as for stratifying patients for clinical trials at international level. The last update by the World Health Organization of CNS tumor classification and grading in 2021 considered, for the first time, *IDH*-wildtype glioblastoma and astrocytoma *IDH*-mutant grade 4 as different tumors. Mutations in the genes isocitrate dehydrogenase (*IDH*) 1 and 2 occur early and, importantly, contribute to gliomagenesis. *IDH* mutation produces a metabolic reprogramming of tumor cells, thus affecting the processes of hypoxia and vascularity, resulting in a clear advantage for those patients who present with *IDH*-mutated astrocytomas. Despite the clinical relevance of *IDH* mutation, current protocols do not include full sequencing for every patient. Alternative biomarkers could be useful and complementary to obtain a more reliable classification. In this sense, magnetic resonance imaging (MRI)-perfusion biomarkers, such as relative cerebral blood volume and flow, could be useful from the moment of presurgery, without incurring additional financial costs or requiring extra effort. The main purpose of this work is to analyze the vascular and hemodynamic differences between *IDH*-wildtype glioblastoma and *IDH*-mutant astrocytoma. To achieve this, we evaluate and validate the association between dynamic susceptibility contrast-MRI perfusion biomarkers and *IDH* mutation status. In addition, to gain a deeper understanding of the vascular differences in astrocytomas depending on the *IDH* mutation, we analyze the transcriptomic bases of the vascular differences.

Abbreviations: BMP2, bone morphogenetic protein 2; CNS, central nervous system; DEGs, differential expressed genes; DSC, dynamic susceptibility contrast; EFEMP2, EGF-containing fibulin-like extracellular matrix protein 2; GO, gene ontology; GSEA, gene set enrichment analysis; HAT, high angiogenic tumor; IDH, isocitrate dehydrogenase; IPE, infiltrated peripheral edema; LAT, low angiogenic tumor; MDK, midkine; MRI, magnetic resonance imaging; MTT, mean transit time; OS, overall survival; rCBF, relative cerebral blood flow; rCBV, relative cerebral blood volume; SLCA10, solute carrier family 2 member 10; TCIA, The Cancer Imaging Archive; TMBIM1, transmembrane BAX inhibitor motif-containing 1; TMM, Trimmed Mean of M-values; VPE, vasogenic peripheral edema; WHO, World Health Organization.

KEYWORDS
astrocytomas grade 4, gene expression, IDH mutation, MRI-DSC biomarkers, vascularity

1 | INTRODUCTION

The last central nervous system (CNS) tumor classifications made by the World Health Organization (WHO)[1,2] classified astrocytomas grade 4 as two different tumors: isocitrate dehydrogenase (*IDH*)-wildtype glioblastoma and *IDH*-mutant astrocytoma grade 4. *IDH* mutations represent the earliest genetic events in gliomagenesis progression, with important implications for diagnosis and therapy. In particular, *IDH* mutations in CNS tumors indicate the transformation from lower-grade gliomas and are associated with better outcomes in high-grade gliomas, indicating the relevance of *IDH* testing.[3] *IDH*-wildtype glioblastoma represents about 95% of grade 4 astrocytomas and predominates in patients who are older than 55 years. Astrocytoma *IDH*-mutant grade 4 (about 5% of cases) is more frequent in younger patients or in those with a history of prior lower-grade diffuse glioma.[1,2,4]

Clinically, these two types of astrocytoma result in different patient survival rates,[4–7] as well as distinct therapy responses.[8–10] Therefore, an early-stage classification considering the *IDH* mutation is necessary to obtain an adequate prognostic evaluation and a more personalized treatment of patients with astrocytomas grade 4.

Sequencing and immunohistochemistry are commonly used to assess the status of *IDH* mutations, but both are invasive because tissue biopsy samples are required. Additionally, the definition of a full *IDH* evaluation can differ according to patient age,[2] clinical protocols, and centers, as reviewed in "The clinical use of IDH1 and IDH2 mutations in gliomas".[11] Sequencing performance differs depending on technique and, in the case of patients who are older than 55 years, suggests that sequencing may not be needed in the setting of negative R132H *IDH1* immunohistochemistry, but non-R132H *IDH1* mutations and *IDH2* mutations are missed.

Because protocols do not include full sequencing for every patient, alternative biomarkers can be useful and complementary to help obtain a more reliable classification. In this sense, magnetic resonance imaging (MRI)-based methodologies could be key because they are noninvasive, can be used from the moment of presurgery, and do not involve additional financial costs or require extra effort. Currently, in clinical practice, the first clinical indication of CNS tumors is radiologically based using the presurgical MR images of the patient. In particular, dynamic susceptibility contrast (DSC) perfusion MRI has shown the capability to identify, characterize, and classify high-grade astrocytomas,[1,2,12–15] evidencing the marked vascular architecture and dynamics of these brain tumors.

In 2020, Wu et al.[12] evaluated the potential clinical impact of DSC perfusion MRI data for predicting *IDH* mutation status in patients with glioma tumors using the ONCOhabitats methodology.[13–15] They analyzed the association between the relative cerebral blood volume (rCBV) in the high angiogenic tumor (HAT) habitat and the *IDH* mutation status. A significantly decreased rCBV for the *IDH*-mutant group was found. They concluded that "the ONCOhabitats method was proven to have high prediction capabilities for *IDH* mutation status in high-grade glioma patients". Despite the great interest in these results, that study only included 25 patients with astrocytoma grade 4. In addition, the molecular basis of these vascular differences between these two high-grade tumors is still unsolved.

The main purpose of this work is to evaluate and validate the association between MRI-DSC biomarkers and *IDH* mutation status in high-grade astrocytomas in a multicenter and international cohort of 299 patients. Additionally, we offer a transcriptomic study to gain a deeper understanding of the vascular differences between these two high-grade astrocytomas. Our results in MRI-DSC show a higher vascularity for *IDH*-wildtype compared with *IDH*-mut astrocytomas grade 4. Transcriptomic results indicate a higher number of differential expressed genes (DEGs) involved in the vascular environment in *IDH*-wildtype tumors (143: CPTAC-3; 123: TCGA), in contrast to *IDH*-mutated tumors (30: CPTAC-3; 37: TCGA). Finally, MRI-DSC perfusion biomarkers (e.g., rCBV and relative cerebral blood flow (rCBF) can detect differences during the presurgical stage of the tumor and then identify *IDH*-mutation status.

2 | MATERIALS AND METHODS

2.1 | Study cohorts

2.1.1 | Patient cohort with MRI data

The study cohort included 299 patients with MRI data, 16 of whom presented with astrocytoma *IDH*-mutant grade 4, and 283 who presented with *IDH*-wildtype glioblastoma, in agreement with the population rates. To collect this cohort, both open (35 patients from TCGA-GBM, 19 patients from Ivy GAP, and 10 from CPTAC-3) and project-specific datasets (108 patients from the MTS4UP dataset, 20 from the GEINO-mol dataset, and 107 from the GLIOCAT dataset), were used. Public datasets are available in The Cancer Imaging Archive (TCIA; https://www.

cancerimagingarchive.net/). Project-specific data are available upon reasonable request to the authors. The ethics committee of Universitat Politècnica de València gave ethical approval for this work.

2.1.2 | Public dataset with RNAseq data

To analyze differences in gene expression between these two types of astrocytoma, two public datasets were used, including 99 patients from CPTAC3 and 151 patients from TCGA-GBM.

2.2 | MRI data

Presurgical MRI data were collected from all the included datasets, including pre- and post-gadolinium T1-weighted, T2-weighted, fluid-attenuated inversion recovery (FLAIR), and DSC T2*-weighted perfusion sequences obtained by the standard of care protocols using 1.5 or 3.0 T.

2.2.1 | MRI processing and perfusion markers calculation

To process the MRIs and to calculate the imaging vascular biomarkers, we used the ONCOhabitats methodology (www.oncohabitats.upv.es).[13–15] ONCOhabitats is illustrated in Figure 1 and includes the following stages:

a. **Preprocessing**. During this stage, common MRI artifacts such as magnetic field inhomogeneities and noise, multimodal registration, brain extraction, or motion correction, are corrected.
b. **Glioma segmentation**. A deep learning 3D convolutional neural network is implemented to segment the enhancing tumor, the edema, and the necrotic tissue. This methodology uses the unenhanced and gadolinium-based contrast agent-enhanced T1-weighted sequences, the T2-weighted sequence, and the FLAIR T2-weighted sequence combined with atlas-based prior knowledge of healthy tissues to delineate the regions.
c. **DSC perfusion quantification**. During this stage, the hemodynamic maps derived from the DSC perfusion sequence are calculated, including rCBV, rCBF, mean transit time (MTT), and K2 permeability. All perfusion maps are normalized against contralateral unaffected white matter volume to achieve consistency and comparability across different datasets. The normalization is performed automatically by a convolutional neural network, which detects the contralateral unaffected white matter region with 90% accuracy. To ensure correct perfusion quantification and to avoid underestimation and overestimation of perfusion markers, DSC perfusion quantification includes a correction for contrast agent

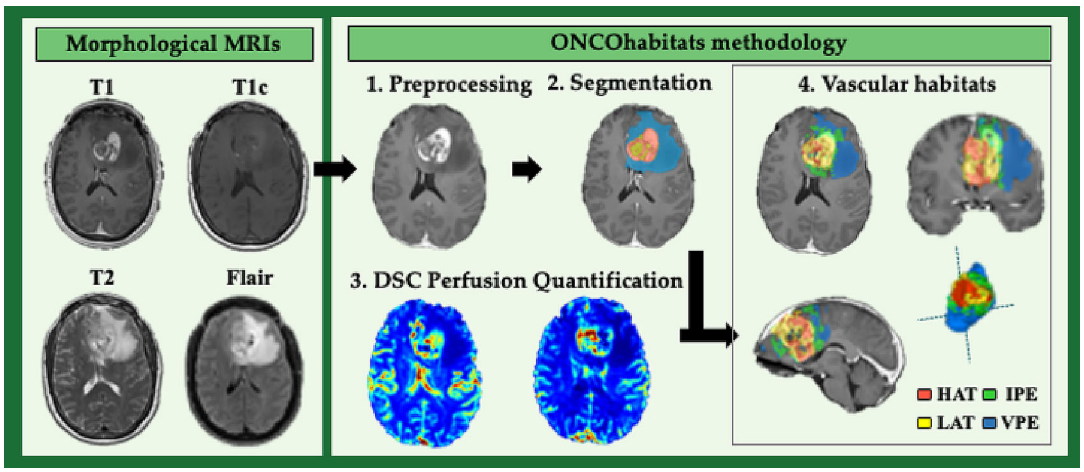

FIGURE 1 The ONCOhabitats methodology includes four stages: (1) preprocessing; (2) glioma segmentation in classical tissues: active tumor, edema, and necrosis; (3) DSC perfusion quantification; and (4) HTS habitats: high angiogenic tumor (HAT), low angiogenic tumor (LAT), infiltrated peripheral edema (IPE), and vasogenic peripheral edema (VPE). DSC, dynamic susceptibility contrast; FLAIR, fluid-attenuated inversion recovery; HTS, hemodynamic tissue signature.

leakage effects. The hemodynamic tissue signature (HTS) method implements the Boxerman leakage-correction method[16] for T1- and T2-leakage effects, as well as gamma-variate fitting to remove the extravasation phase and second pass of the contrast bolus.

d. **Vascular habitats.** During this final stage, the four vascular habitats within the tumor and edema are delineated by a directional class adaptive spatially varying finite mixture model (DCA-SVFMM), which is a clustering algorithm that combines Gaussian mixture modeling with continuous Markov random fields to make use of the self-similarity and local redundancy of the images. Each delineated habitat presents its specific hemodynamic behavior. They are named as: the high angiogenic tumor (HAT) habitat, the low angiogenic tumor (LAT) habitat, the infiltrated peripheral edema (IPE) habitat, and the vasogenic peripheral edema (VPE) habitat. Vascular habitats are delineated using a DCA-SVFMM structured clustering of rCBV and rCBF maps. The clustering includes two stages: (i) a two-class clustering of the whole enhancing tumor and edema regions; and (ii) a two-class clustering performed by using only the rCBV and rCBF data within the regions obtained in the first stage. To ensure the reproducibility of the HTS, both stages are initialized with a deterministic seed method.

2.3 | RNA data

2.3.1 | Data download and normalization

For both open datasets, we retrieved the HT-Seq mRNA read counts from the TCGA database. Samples without *IDH* status information were filtered out to define two experimental groups: *IDH*-mutant and *IDH*-wildtype. Read counts were filtered by expression, removing genes with low counts across all samples. Normalization factors were calculated for each dataset using the Trimmed Mean of M-values (TMM) method.[17]

2.3.2 | Differential gene expression analysis

We determined the DEGs in both datasets by fitting a quasi-likelihood negative binomial generalized log-linear model, implemented in the *edgeR* R package.[17] *p* values were corrected using the Benjamini–Hochberg procedure to control type I errors when conducting multiple comparisons. Genes having an adjusted *p* value lower than 0.05 and an absolute value of log fold-change greater than 1 were considered differentially expressed.

2.4 | Statistical analyses

2.4.1 | Study cohort description

To evaluate the differences in survival between both groups of patients, Kaplan–Meier analyses and log rank tests were performed. The relationships between demographic and clinical variables, and overall survival (OS), were assessed using independent uniparametric Cox regression models.

2.4.2 | Correlation between MRI-DSC biomarkers calculated at vascular habitats with *IDH*-mutation status

We evaluated the significant correlation between each MRI-DSC biomarker with OS to select the optimal biomarkers to find differences among astrocytoma types.

Differences in the imaging vascular biomarkers between *IDH*-wildtype glioblastoma and *IDH*-mutant astrocytoma grade 4 were assessed with the Mann–Whitney U test, and boxplots were performed to illustrate differences.

2.4.3 | Differences in transcriptome between high-grade astrocytoma types

Results from differential expression analysis were functionally annotated using the Biological Processes ontology from the Gene Ontology (GO) database.[18,19] First, we selected the GO terms related to vascular processes by matching a list of vascular key terms (Table S1). Then we selected all genes mapping with these matched GO terms as our vascular genes set. The most significant vascular and nonvascular DEGs were plotted in heatmaps to illustrate the differences between expression profiles across the experimental groups.

Finally, we assessed overall functional differences between astrocytoma types by performing gene set enrichment analysis (GSEA) on differential expression analysis results using the *fgsea* R package.[19] Genes were preranked according to their log fold-change values. Gene sets with an adjusted *p* value of less than 0.05 were considered significant.

3 | RESULTS

3.1 | Detection of relevant prognostic demographic and clinical variables

We analyzed the correlation between OS with the following demographic and clinical characteristics: age, sex, tumor resection type, tumor location (hemisphere), *IDH* mutation, and *MGMT* methylation. The results are provided in Figure 2A, showing the *IDH* mutation as the variable most correlated with longer survival rates (with the lowest hazard ratio), followed by methylated *MGMT* and total tumor resection.

3.2 | Cohort descriptions

The proportions of each type of astrocytoma in this study dataset are compatible with previously published literature,[1,2,12,13] representing the population with *IDH*-wildtype glioblastoma as 95% of the entire cohort (Figure 2B). In addition, the number of patients from each dataset with *IDH*-mutant astrocytoma and *IDH*-wildtype glioblastoma were compared, showing the differences in proportions among the datasets (Figure 2C).

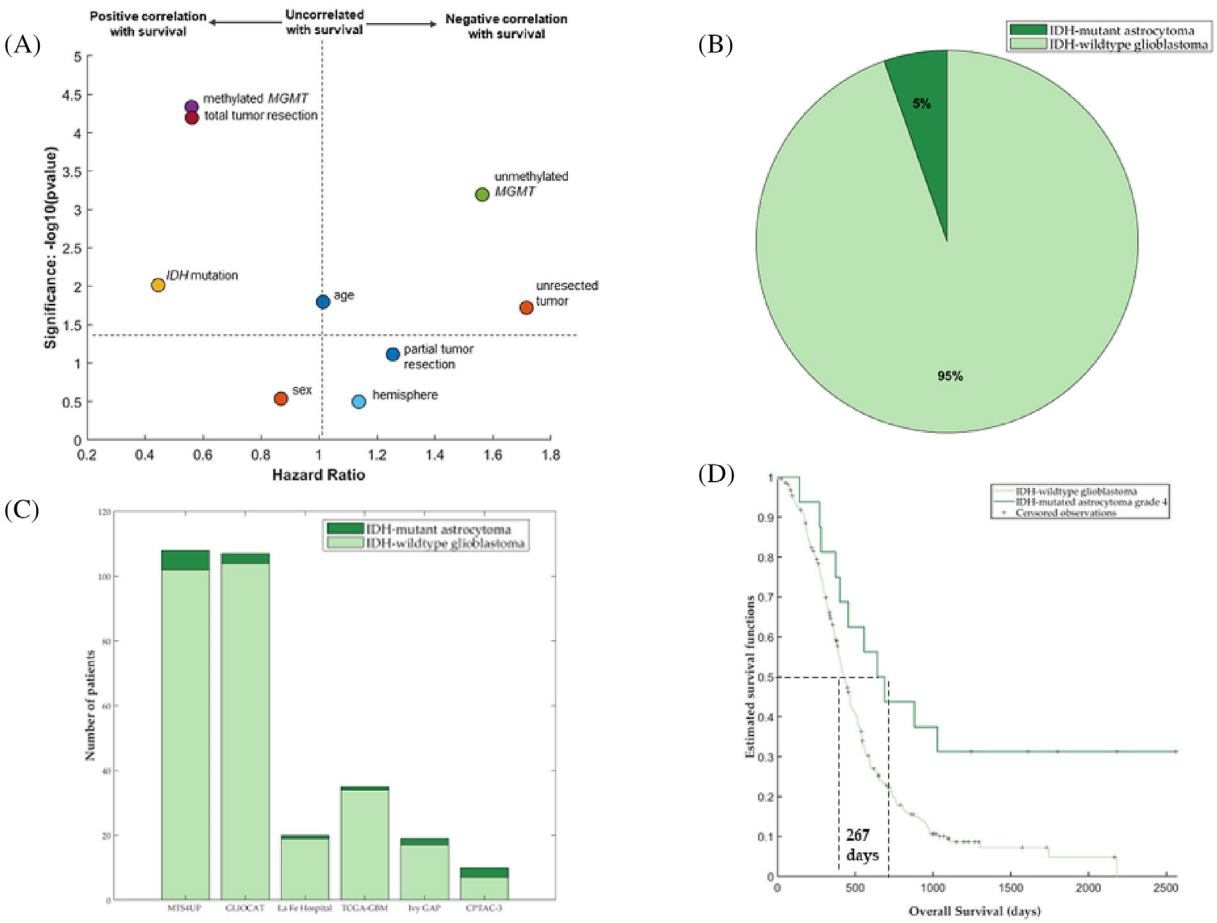

FIGURE 2 (A) Scatter plot with the correlation between the main demographic and clinical characteristics and overall survival (OS). (B) Proportion of patients of the studied cohort with *IDH*-mutant astrocytoma and *IDH*-wildtype glioblastoma. (C) Number of patients from each dataset with MRI data. (D) Kaplan–Meier curves showing the survival differences between patients with astrocytoma *IDH*-mutant grade 4 (n = 16) and glioblastoma *IDH*-wildtype (n = 287). The median OS between these two groups was 267 days.

TABLE 1 Demographic, clinical, and molecular features for the cohort with *IDH*-mutant astrocytoma (n = 16) and for the cohort with *IDH*-wildtype glioblastoma (n = 287). *p* values resulting from the Mann–Whitney test are also included.

	IDH-mutant astrocytoma grade 4	*IDH*-wildtype glioblastoma	*p* values (Mann–Whitney test)
# patients (% of entire cohort)	16 (5.3%)	287 (94.7%)	-
Sex (#, % females)	9 (56.2%)	101 (35.2%)	0.1339
Mean age at diagnosis (years)	49	60	0.0007*
Resection type (# patients)			
- Total	5 (31.2%)	92 (32.1%)	0.9183
- Partial	6 (37.5%)	122 (42.5%)	0.6609
- Biopsy	0 (0.0%)	24 (8.4%)	0.2265
- Unknown	5 (31.2%)	49 (17.1%)	0.1106
MGMT methylation (# patients; %)			
-Methylated	6 (37.5%)	93 (32.4%)	0.7032
-Unmethylated	5 (31.2%)	111 (38.7%)	0.5262
-Unknown	5 (31.2%)	83 (28.9%)	0.7746

*p-value < 0.05.

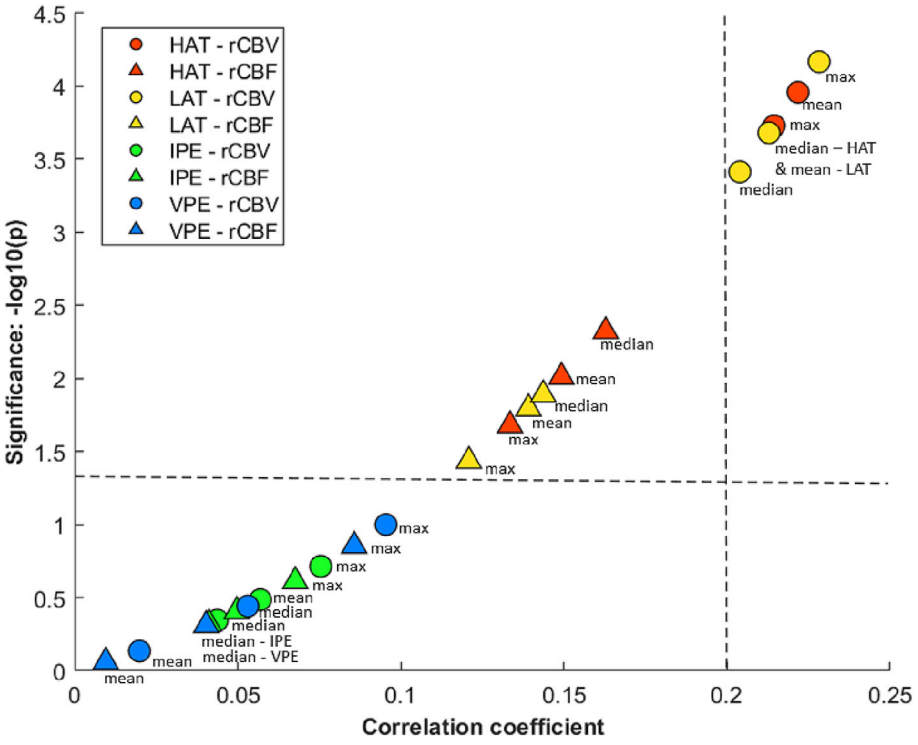

FIGURE 3 Scatter plot with the correlation results (Spearman coefficients and significance) between MRI-DSC biomarkers and overall survival for the entire cohort (n = 299). Circles show rCBV and triangles show rCBF. Each habitat is represented by a color, HAT in red, LAT in yellow, IPE in green, and VPE in blue, and different metrics are also indicated (mean, median, and maximum). DSC, dynamic susceptibility contrast; HAT, high angiogenic tumor; IPE, infiltrated peripheral edema; LAT, low angiogenic tumor; rCBF, relative cerebral blood flow; rCBV, relative cerebral blood volume; VPE, vasogenic peripheral edema.

Differences in OS between these two groups were studied, demonstrating significantly longer survival times for the group of patients with *IDH*-mutant astrocytoma grade 4 ($p = 0.001$, log-rank test). Kaplan–Meier curves are included in Figure 2D, illustrating a median difference in OS of 267 days between the two populations.

Differences in the main demographic, clinical, and molecular features between the two populations were analyzed and the results are included in Table 1.

Only the median age of diagnosis was significantly different between the groups, being lower for the group of patients with astrocytoma *IDH*-mutant grade 4 (age, 49 vs. 60 years).

3.3 | Correlation between imaging vascular biomarkers and overall survival

rCBV and rCBF markers at each vascular habitat (HAT, LAT, IPE, and VPE) and for each metric (mean, median, and maximum) were calculated, resulting in 24 image markers. We studied the potential prognostic capacity of these markers, analyzing their correlation with *IDH* mutational status.

Figure 3 shows the correlation coefficient and the significance of each MRI-DSC biomarker with overall survival. We can see that the 12 markers related to the HAT and LAT habitats are the most significantly correlated ($p < 0.05$), but only the rCBV markers yield a coefficient higher than 0.2. The selected markers to develop the following analyses were HAT-rCBV$_{mean}$, HAT-rCBV$_{median}$, HAT-rCBV$_{max}$, LAT-rCBV$_{mean}$, LAT-rCBV$_{median}$, and LAT-rCBV$_{max}$.

Significant differences (Mann–Whitney test, $p < 0.05$) in the selected imaging vascular biomarkers between *IDH*-mutant astrocytoma grade 4 and *IDH*-wildtype glioblastomas were found and are illustrated in Figure 4. For all the selected MRI-DSC markers, the median value and the minimum and maximum range were higher for the *IDH*-wildtype glioblastoma group, suggesting significantly higher vascularity for these tumors in comparison with those in the *IDH*-mutant astrocytoma grade 4 group. Table S2 includes the exact values of each biomarker for the group of *IDH*-wildtype glioblastoma and that of *IDH*-mutant astrocytoma grade 4.

3.4 | Distinct transcriptome between *IDH*-wildtype glioblastoma and *IDH*-mutant astrocytoma grade 4

Differential expression analysis revealed considerable transcriptomic variations between *IDH*-wildtype glioblastoma and astrocytoma *IDH*-mutant grade 4. The total number of significant DEGs (adjusted p value < 0.05 and absolute log fold-change > 1) was consistent across datasets (2568 and 2056 DEGs from CPTAC-3 and TCGA, respectively, with an intersection of 879 DEGs).

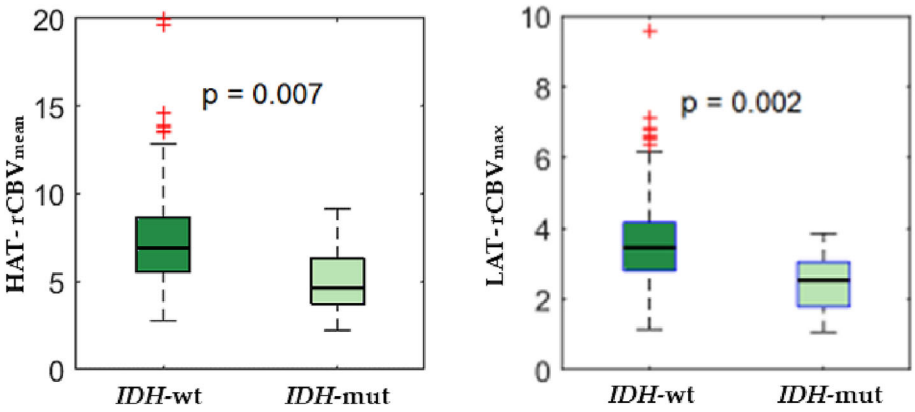

FIGURE 4 Boxplot showing differences in MRI-DSC biomarkers (at high and low angiogenic tumor habitats) between glioblastomas *IDH*-wildtype and astrocytomas *IDH*-mutant grade 4. DSC, dynamic susceptibility contrast; HAT, high angiogenic tumor; LAT, low angiogenic tumor; mut, mutant; rCBV, relative cerebral blood volume; wt, wildtype.

TABLE 2 Intersection of differential expressed genes labeled as "vascular" between the CPTAC-3 and TCGA datasets.

Overexpressed in	Significant genes
IDH-wildtype glioblastoma	ADAM12, ADAMTS1, ADORA1, ADRB1, AK4, ANXA1, BCL3, C1QTNF1, CCL28, CDKN1A, CHI3L1, CHST2, CLDN1, CLIC1, COL1A1, COL3A1, CREB3L1, CSRP1, CUL7, CYGB, DBH, DCN, DPP4, EDA2R, EFEMP2, EFNB2, EMILIN2, EMP2, EPHA2, ERBB2, ERRFI1, F3, FABP5, FGF1, FOXJ1, FZD6, GRB10, HOXA1, IL27RA, ITGA5, LMNA, LOXL1, MDK, MEOX2, MMP14, MT3, MYL12A, MYL9, NOS2, NPNT, NR2E1, P2RY1, PCSK5, PDGFA, PDLIM1, PDPN, PLAT, PLK2, PLOD3, PTK2B, RHOJ, SCNN1B, SERPING1, SLC27A1, SLC2A10, SLC4A3,SOCS3, SPON2, SPRY2, STRA6, TERT, TMBIM1, VASN, VAV3, WWTR1
Astrocytoma *IDH*-mutant grade 4	ANGPT4, BMP2, CELA2A, CRYAB, EYA1, NOG, PGF, SGCD, STOX1, TACR1, TMEM100

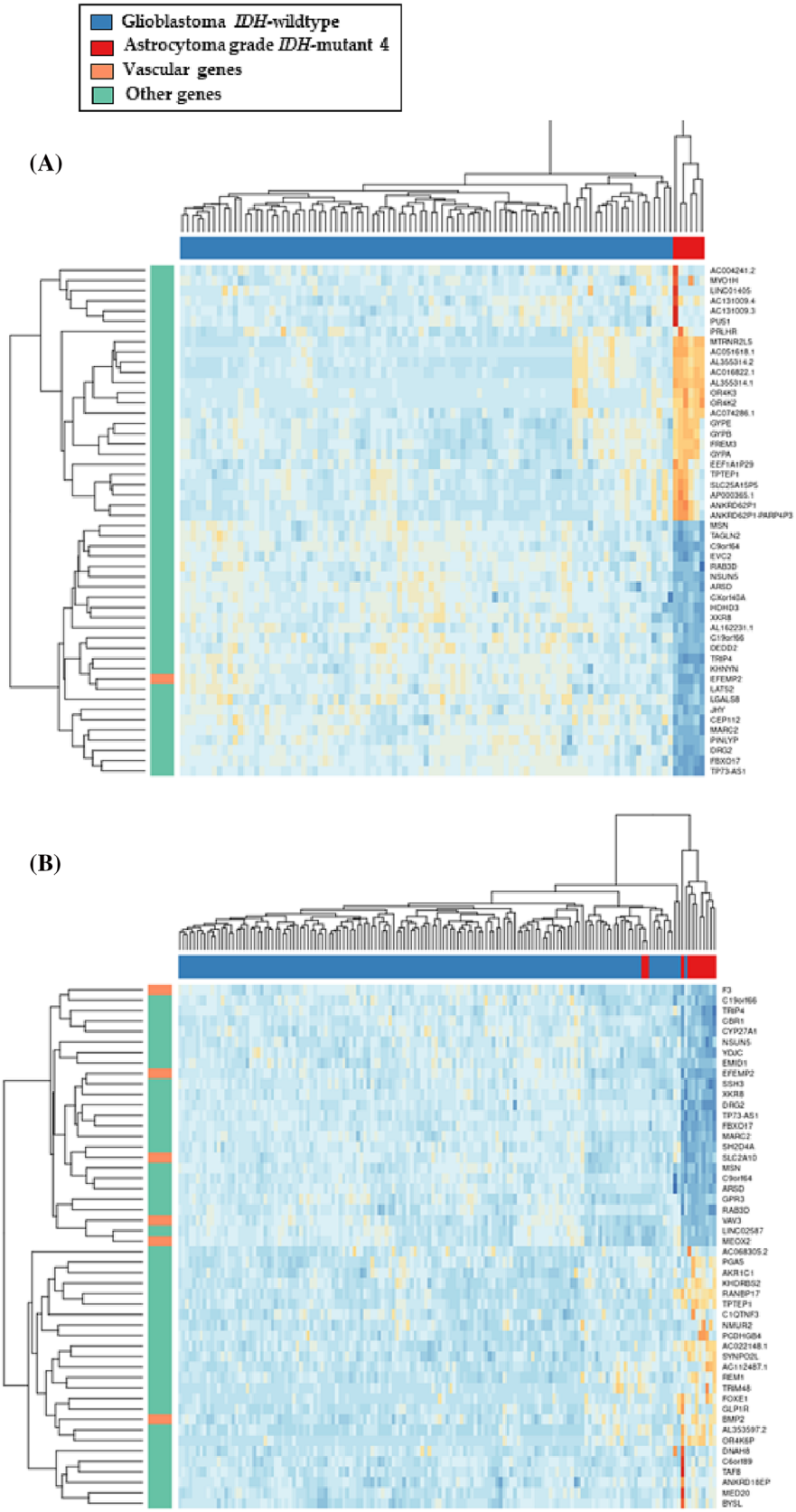

FIGURE 5 Heatmaps showing different gene expressions between *IDH*-wildtype glioblastoma (blue) and *IDH*-mutant astrocytoma grade 4 (red) were created with the two open datasets: (A) CPTAC-3 (n = 93 IDH-wt, and n = 6 *IDH*-mut, respectively); and (B) TCGA-GBM (n = 140 *IDH*-wt, and n = 11 *IDH*-mut, respectively). mut, mutant; wt, wildtype.

We detected 1313 (CPTAC-3) and 1262 (TCGA) overexpressed genes in the *IDH*-wildtype group. A considerable fraction of these DEGs were considered part of the "vascular" functional gene set (143 and 123, respectively, with an intersection of 75 DEGs, as reported in Table 2).

Also, we determined that a total of 1345 (CPTAC-3) and 794 (TCGA) genes were overexpressed in the *IDH*-mutant group. A total of 30 and 37 DEGs, respectively, were labeled as "vascular" genes, having in common a group of 11 DEGs (Table 2).

Figure 5 consists of the heatmaps showing different gene expressions between *IDH*-wildtype glioblastoma and astrocytoma *IDH*-mutant grade 4 performed with the two open datasets. Vascular genes are marked in different colors.

All significant DEGs, labeled as vascular or nonvascular, are included in Table S3. This table also contains the adjusted *p* values and the log fold-change values for each gene.

The GSEA results showed significant differences between the two groups at the biological process level. On the one hand, a total of 169 (CPTAC-3) and 39 (TCGA) GO terms showed significant overrepresentation in IDH-wildtype glioblastomas. Among them, 13 (CPTAC-3) and two (TCGA) GO terms were implicated in vascular processes (Figure 6).

On the other hand, we only detected one (CPTAC-3) and three (TCGA) significantly overrepresented GO terms in *IDH*-mutated astrocytomas. There was not any coincident function between sets. Moreover, none of these significant functions were related to any "vascular" term.

3.5 | Combined transcriptomic and imaging analysis differentiate between glioblastoma *IDH*-wildtype and astrocytoma *IDH*-mutant grade 4

We studied the combined information that provided the analyses of both transcriptomic and imaging data. Figure 7 includes a heatmap with the top genes enriched and the MRI-DSC biomarkers for seven patients from the public database CPTAC-3 (which includes both imaging and transcriptomic data).

We can see that, although not generalizable for all the cases, patients with *IDH*-wildtype glioblastoma appear to present with higher values of the MRI-DSC perfusion biomarkers than those with astrocytoma *IDH*-mutant grade 4.

These results should be considered with caution because of the low number of patients included in the analyses.

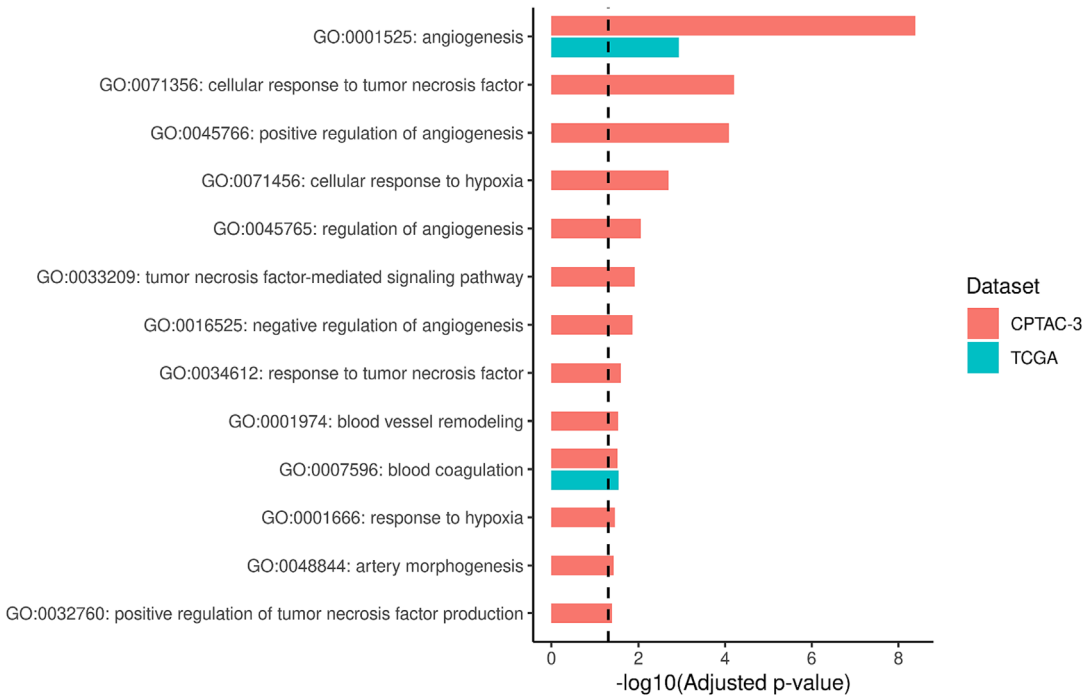

FIGURE 6 Significantly overrepresented GO terms (from Biology Processes Ontology) related to vascular functions in glioblastoma *IDH*-wildtype. GSEA results obtained for the CPTAC-3 dataset (red bars) and the TCGA dataset (blue bars). GO, gene ontology; GSEA, gene set enrichment analysis.

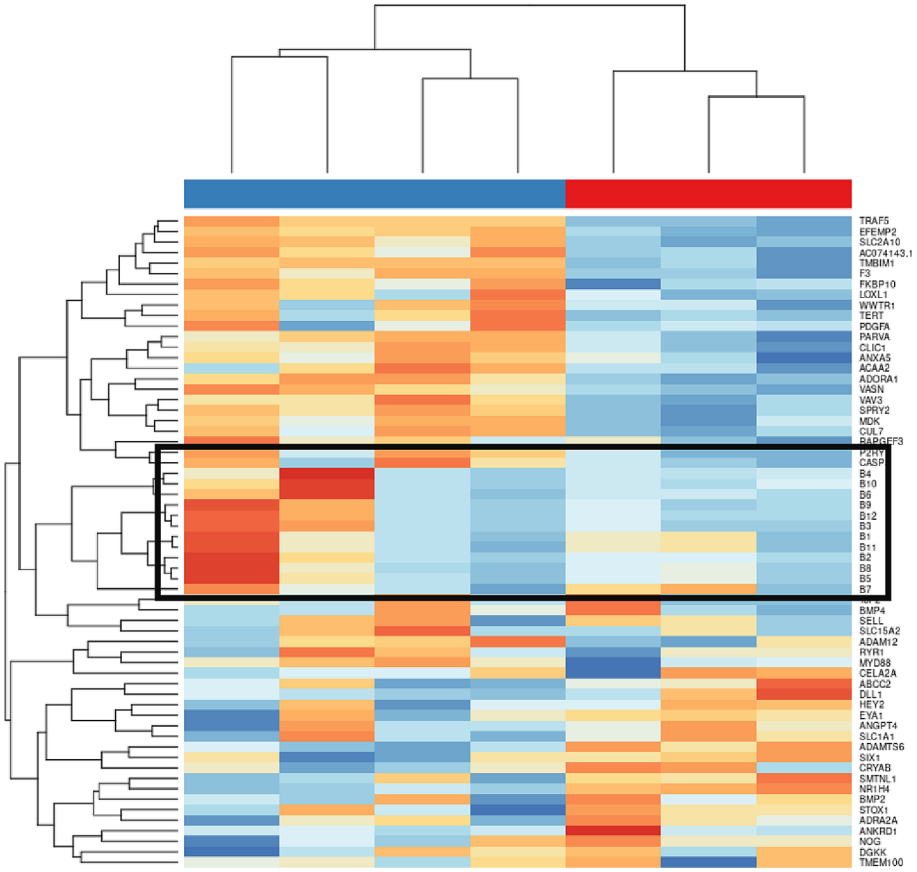

FIGURE 7 Heatmap showing differences in gene expressions and in MRI-DSC biomarkers between glioblastoma *IDH*-wildtype (n = 4) and astrocytoma *IDH*-mutant grade 4 (n = 3). Data were extracted from the public database CPTAC3. B1: mean rCBV at HAT; B2: median rCBV at HAT,: B3: maximum rCBV at HAT; B4: mean rCBF at HAT; B5: median rCBF at HAT,: B6: maximum rCBF at HAT; B7: mean rCBV at LAT; B8: median rCBV at LAT; B9: maximum rCBV at LAT; B10: mean rCBF at LAT; B11: median rCBF at LAT; B12: maximum rCBV at LAT. DSC, dynamic susceptibility contrast. HAT, high angiogenic tumor; LAT, low angiogenic tumor; rCBF, relative cerebral blood flow; rCBV, relative cerebral blood volume.

4 | DISCUSSION

In the current study, we have demonstrated that *IDH*-wildtype glioblastoma and *IDH*-mutant astrocytoma grade 4 present different vascular patterns, both in high- and low-angiogenic tumor habitats, as defined by the automatic ONCOhabitats methodology.[13–15] These differences can be detected using MRI-DSC biomarkers, such as rCBV and rCBF, calculated from the presurgical stage, because they are correlated with the *IDH* mutation status of the tumor. These results were obtained with a multicenter cohort of 299 patients and validate those reported in a previous study.[13]

The correlation among gene expression levels related to angiogenesis and perfusion parameters in glioblastoma has been explored in several earlier studies.[20–26] Additionally, the correlation of perfusion parameters and angiogenesis gene expression has been shown in several cancers, indicating their relevance in patient diagnosis and prognosis.[27–29]

Angiogenesis and tumor vasculature support tumor progression.[29] The association between tumor and edema vascularity and survival has been previously analyzed in the literature.[14,15,30] There is a consensus that higher values of vascularity, measured by DSC-MRI biomarkers, result in shorter survival times. These important differences in patient survival may be due in part to different vascular behavior, resulting in quicker progression and greater aggressiveness of *IDH*-wildtype glioblastomas.[31–33] With this work, we have validated this hypothesis, demonstrating significantly higher rCBV values for *IDH*-wildtype glioblastomas. The clinical relevance of this finding provides an opportunity to use the DSC-MRI biomarkers as complementary tools to support the first clinical indication made by the radiologist from the presurgical stage and prognosis information. Additionally, DSC-MRI biomarkers may overcome the limitations of conventional imaging methods in antiangiogenic trials because they support information on vascular permeability, blood flow, and blood volume, among others.

In addition, to acquire a deeper understanding of vascular differences between these two high-grade astrocytomas, we analyzed gene expression patterns of two public datasets that include RNAseq data. We focused on analyzing genes related to vascular processes and structures. We

found that 75 genes related to vascularity were upregulated in both datasets for the group of *IDH*-wildtype glioblastoma, versus only 11 vascular genes upregulated in the group of *IDH*-mutant astrocytoma grade 4. This finding supports our hypothesis that stronger vascular processes occur during the establishment and progression of *IDH*-wildtype tumors.

In glioblastomas *IDH*-wildtype, we found overexpression of several genes previously reported as associated with vascular remodeling and arterial abnormalities in high-grade gliomas. Some of these genes are *EGF-containing fibulin-like extracellular matrix protein 2 (EFEMP2)*,[34] *solute carrier family 2 member 10 (SLC2A10)*,[35] *midkine (MDK)*,[36] and *transmembrane BAX inhibitor motif-containing 1 (TMBIM1)*.[37] They also have been proven as associated with poor progression, which seems coherent because a higher vascular supply allows quicker tumor progression.

On the other hand, there were 11 vascular genes overexpressed in astrocytomas *IDH*-mutated grade 4 compared with glioblastomas *IDH*-wildtype. We can comment on the relevance of *bone morphogenetic protein 2 (BMP2)*, which has been previously defined as relevant for prognosis estimation,[38] because the higher the expression of *BMP2*, the better the prognosis of patients. In addition, we found an overexpression in *STOX1*, which was previously associated with younger patients and with gliomas of a lower grade that are less aggressive.[39] The correlation of higher expression of these genes with the presence of *IDH* mutation can be attributed to the metabolic reprogramming that tumor cells undergo with this alteration.

Furthermore, an observational analysis of the combined analysis of gene expression and MRI-DSC biomarkers suggests that imaging data can contribute to the improvement of models for differentiating these tumors. Vascular differences that present at gene expression level appear to be detected with MRI from the first stage of diagnosis. These results are preliminary, and they must be validated with larger cohorts that include both imaging and transcriptomic data. However, this study opens possibilities to propose DSC-MRI biomarkers as useful for an early and noninvasive estimation of *IDH* mutation in patients with astrocytoma grade 4.

The available literature indicates that DSC-derived biomarkers are a valuable and potentially essential complement to standard MRI. However, some experts have suggested that the clinical adoption of DSC-derived biomarkers is restricted because of a lack of standardization, which may account for the variations in reported rCBV and rCBF thresholds. Nonetheless, recent studies have demonstrated the exceptional reproducibility, consistency across different sites, and commercial availability of carefully curated DSC quantification protocols,[40] indicating a high level of technological readiness for this technique.[41] The adoption of standardized protocols by the MR community will enhance the reliability of the DSC-derived biomarkers and their suitability for clinical use.

Our study revealed significant dissimilarities between DSC-derived markers in *IDH*-wildtype and *IDH*-mutant tumors, specifically in grade 4 astrocytomas. Nonetheless, generalization of these findings to lower-grade gliomas or other brain tumor subtypes with limited angiogenic activity may not be feasible.

5 | CONCLUSIONS

In the current study, we have validated the association between *IDH* mutation and tumor vascularity as measured by DSC-MRI biomarkers in high- and low-angiogenic habitats of astrocytomas grade 4. Astrocytomas of *IDH*-mutant grade 4 present lower rCBV and rCBF, and longer survival times, which can be partly explained by slower tumor progression resulting from lower vascularity.

We have assessed the potential relevance of specific genes overexpressed in glioblastomas *IDH*-wildtype, such as *EFEMP2*, *SLC2A10*, *MDK*, and *TMBIM1*, and in *IDH*-mutant astrocytoma grade 4, such as *BMP2* and *STOX1*. Although more in-depth analyses are needed, these genes can be proposed as targets for specific novel therapies for each type of high-grade astrocytoma.

This constitutes the first study to analyze vascular differences at both MRI and transcriptomic level between *IDH*-wildtype glioblastoma and *IDH*-mutant astrocytoma grade 4. We propose that DSC-MRI biomarkers automatically calculated with the ONCOhabitats method should be used to estimate the *IDH* mutation status in grade 4 astrocytomas from the presurgical stage onwards. Moreover, we suggest the key role of specific genes overexpressed in *IDH*-wildtype glioblastoma as a determinant for presenting stronger vascularity; and the clinical relevance of *BMP2* and *STOX1* for *IDH*-mutant astrocytoma grade 4.

CONFLICT OF INTEREST STATEMENT

The authors declare that there is no conflict of interest.

REFERENCES

1. Louis DN, Perry A, Wesseling P, et al. The 2021 WHO classification of tumors of the central nervous system: A summary. *Neuro Oncol*. 2021;23(8):1231-1251. doi:10.1093/neuonc/noab106
2. Louis DN, Perry A, Reifenberger G, et al. The 2016 World Health Organization Classification of Tumors of the Central Nervous System: a summary. *Acta Neuropathol*. 2016;131(6):803-820. doi:10.1007/s00401-016-1545-1
3. Dang L, Jin S, Su SM. IDH mutations in glioma and acute myeloid leukemia. *Trends Mol Med*. 2010;16(9):387-397. doi:10.1016/j.molmed.2010.07.002
4. Ohgaki H, Kleihues P. The definition of primary and secondary glioblastoma. *Clin Cancer Res*. 2013;19(4):764-772. doi:10.1158/1078-0432.CCR-12-3002

5. Yan H, Parsons DW, Jin G, et al. IDH1 and IDH2 mutations in gliomas. *N Engl J Med*. 2009;360(8):765-773. doi:10.1056/NEJMoa0808710
6. Mirchia K, Richardson TE. Beyond IDH-mutation: Emerging molecular diagnostic and prognostic features in adult diffuse gliomas. *Cancer*. 2020;12(7):1-22. doi:10.3390/cancers12071817
7. Christians A, Adel-Horowski A, Banan R, et al. The prognostic role of IDH mutations in homogeneously treated patients with anaplastic astrocytomas and glioblastomas. *Acta Neuropathol Commun*. 2019;7(1):156. doi:10.1186/s40478-019-0817-0
8. Opovici-Muller J, Lemieux RM, Artin E, et al. Discovery of AG-120 (Ivosidenib): A first-in-class mutant IDH1 inhibitor for the treatment of IDH1 mutant cancers. *ACS Med Chem Lett*. 2018;9(4):300-305. doi:10.1021/acsmedchemlett.7b00421
9. Kaminska B, Czapski B, Guzik R, Król SK, Gielniewski B. Consequences of IDH1/2 mutations in gliomas and an assessment of inhibitors targeting mutated IDH proteins. *Molecules*. 2019;24(5):968. doi:10.3390/molecules24050968
10. Han S, Liu Y, Cai SJ, et al. IDH mutation in glioma: molecular mechanisms and potential therapeutic targets. *Br J Cancer*. 2020;122(11):1580-1589. doi:10.1038/s41416-020-0814-x
11. Picca A, Berzero G, Di Stefano AL, Sanson M. The clinical use of IDH1 and IDH2 mutations in gliomas. *Expert Rev Mol Diagn*. 2018;18(12):1041-1051. doi:10.1080/14737159.2018.1548935
12. Wu H, Tong H, Du X, et al. Vascular habitat analysis based on dynamic susceptibility contrast perfusion MRI predicts IDH mutation status and prognosis in high-grade gliomas. *Eur Radiol*. 2020;30(6):3254-3265. doi:10.1007/s00330-020-06702-2
13. Juan-Albarracín J, Fuster-Garcia E, García-Ferrando GA, García-Gómez JM. ONCOhabitats: A system for glioblastoma heterogeneity assessment through MRI. *Int J Med Inform*. 2019;128:53-61. doi:10.1016/j.ijmedinf.2019.05.002
14. del Álvarez-Torres MM, Juan-Albarracín J, Fuster-Garcia E, et al. Robust association between vascular habitats and patient prognosis in glioblastoma: An international multicenter study. *J Magn Reson Imaging*. 2020;51(5):1478-1486. doi:10.1002/jmri.26958
15. Juan-Albarracín J, Fuster-Garcia E, Pérez-Girbés A, et al. Glioblastoma: Vascular habitats detected at preoperative dynamic susceptibility-weighted contrast-enhanced perfusion MR imaging predict survival. *Radiology*. 2018;287(3):944-954. doi:10.1148/radiol.2017170845
16. Boxerman JL, Schmainda KM, Weisskoff RM. Relative Cerebral Blood Volume Maps Corrected for Contrast Agent Extravasation Significantly Correlate with Glioma Tumor Grade, Whereas Uncorrected Maps Do Not. Accessed February 2023. www.ajnr.org
17. Robinson MD, Oshlack A. A Scaling Normalization Method for Differential Expression Analysis of RNA-Seq Data; 2010. Accessed February 2023. http://genomebiology.com/2010/11/3/R25 10.1186/gb-2010-11-3-r25
18. Robinson MD, McCarthy DJ, Smyth GK. edgeR: A Bioconductor package for differential expression analysis of digital gene expression data. *Bioinformatics*. 2009;26(1):139-140. doi:10.1093/bioinformatics/btp616
19. Korotkevich G, Sukhov V, Budin N, Shpak B, Artyomov MN, Sergushichev A. *Fast Gene Set Enrichment Analysis*. doi:10.1101/060012
20. Hong XY, Wang J, Li Z. AGR2 expression is regulated by HIF-1 and contributes to growth and angiogenesis of glioblastoma. *Cell Biochem Biophys*. 2013;67(3):1487-1495. doi:10.1007/s12013-013-9650-4
21. Jain R, Poisson L, Narang J, et al. Correlation of perfusion parameters with genes related to angiogenesis regulation in glioblastoma: a feasibility study. *Am J Neuroradiol*. 2012;33(7):1343-1348. doi:10.3174/ajnr.A2956
22. Jain R, Poisson LM, Gutman D, et al. Outcome prediction in patients with glioblastoma by using imaging, clinical, and genomic biomarkers: Focus on the nonenhancing component of the tumor. *Radiology*. 2014;272(2):484-493. doi:10.1148/radiol.14131691
23. Auf G, Jabouille A, Guérit S, et al. Inositol-requiring enzyme 1alpha is a key regulator of angiogenesis and invasion in malignant glioma. *Proc Natl Acad Sci U S A*. 2010;107(35):15553-15558. doi:10.1073/pnas.0914072107
24. Narang J, Jain R, Scarpace L, et al. Tumor vascular leakiness and blood volume estimates in oligodendrogliomas using perfusion CT: an analysis of perfusion parameters helping further characterize genetic subtypes as well as differentiate from astroglial tumors. *J Neurooncol*. 2011;102:287-293. doi:10.1007/s11060-010-0317-3
25. Jain R, Poisson L, Narang J, et al. Genomic mapping and survival prediction in glioblastoma: molecular subclassification strengthened by hemodynamic imaging biomarkers. *Radiology*. 2013;267(1):212-220. doi:10.1148/radiol.12120846
26. Barajas RF Jr, Phillips JJ, Vandenberg SR, et al. Pro-angiogenic cellular and genomic expression patterns within glioblastoma influences dynamic susceptibility weighted perfusion MRI. *Clin Radiol*. 2015;70(10):1087-1095. doi:10.1016/j.crad.2015.03.006
27. Yeo DM, Oh SN, Jung CK, et al. Correlation of dynamic contrast-enhanced MRI perfusion parameters with angiogenesis and biologic aggressiveness of rectal cancer: Preliminary results. *J Magn Reson Imaging*. 2015;41(2):474-480. doi:10.1002/jmri.24541
28. Kambadakone A, Yoon SS, Kim TM, et al. CT perfusion as an imaging biomarker in monitoring response to neoadjuvant bevacizumab and radiation in soft-tissue sarcomas: comparison with tumor morphology, circulating and tumor biomarkers, and gene expression. *Am J Roentgenol*. 2015;204(1):W11-W18. doi:10.2214/AJR.13.12412
29. Ling S, Deng D, Mo Y, Zhang X, Guan X, Wei Q. Correlations between CT perfusion parameters and vascular endothelial growth factor expression and microvessel density in implanted VX2 lung tumors. *Cell Biochem Biophys*. 2014;70(1):629-633. doi:10.1007/s12013-014-9966-8
30. de Palma M, Biziato D, Petrova TV. Microenvironmental regulation of tumour angiogenesis. *Nat Rev Cancer*. 2017;17(8):457-474. doi:10.1038/nrc.2017.51
31. Folkman J. Tumor angiogenesis: Therapeutic implications. *N Engl J Med*. 1971;285(21):1182-1186. doi:10.1056/NEJM197111182852108
32. Weis SM, Cheresh DA. Tumor angiogenesis: Molecular pathways and therapeutic targets. *Nat Med*. 2011;17(11):1359-1370. doi:10.1038/nm.2537
33. Wang L, Chen Q, Chen Z, et al. EFEMP2 is upregulated in gliomas and promotes glioma cell proliferation and invasion. *Int J Clin Exp Pathol*. 2015;8(9):10385-10393.
34. Cheng CH, Kikuchi T, Chen YH, et al. Mutations in the SLC2A10 gene cause arterial abnormalities in mice. *Cardiovasc Res*. 2009;81(2):381-388. doi:10.1093/cvr/cvn319
35. Filippou PS, Karagiannis GS, Constantinidou A. Midkine (MDK) growth factor: a key player in cancer progression and a promising therapeutic target. *Oncogene*. 2020;39(10):2040-2054. doi:10.1038/s41388-019-1124-8
36. Gao L, Liu J, Zhang S, et al. TMBIM1 promotes EMT by stimulating autophagic degradation of E-cadherin via AMPK/mTOR/ULK1 axis in human gliomas. Published Online 2022. doi:10.21203/rs.3.rs-1403508/v2
37. Zhou K, Zhao Z, Li S, Liu Y, Li G, Jiang T. A new glioma grading model based on histopathology and Bone Morphogenetic Protein 2 mRNA expression. *Sci Rep*. 2020;10(1):18420. doi:10.1038/s41598-020-75574-9

38. Jin FQ, Jin L, Wang YL. Downregulation of STOX1 is a novel prognostic biomarker for glioma patients. *Open Life Sci*. 2021;16(1):1164-1174. doi:10.1515/biol-2021-0119
39. Boxerman JL, Quarles CC, Hu LS, et al. Jumpstarting Brain Tumor Drug Development Coalition Imaging Standardization Steering Committee Consensus recommendations for a dynamic susceptibility contrast MRI protocol for use in high-grade gliomas. *Neuro Oncol*. 2020;22:1262-1275. doi:10.1093/neuonc/noaa141
40. Hirschler L, Sollmann N, Schmitz-Abecassis B, et al. Advanced MR techniques for preoperative glioma characterization: Part 1. *J Magn Reson Imaging*. 57(6):1655-1675. doi:10.1002/jmri.28662
41. Hangel G, Schmitz-Abecassis B, Sollmann N, et al. Advanced MR techniques for preoperative glioma characterization: Part 2. *J Magn Reson Imaging*. 57(6):1676-1695. doi:10.1002/jmri.28663

SUPPORTING INFORMATION

Additional supporting information can be found online in the Supporting Information section at the end of this article.

How to cite this article: Álvarez-Torres MM, López-Cerdán A, Andreu Z, et al. Vascular differences between *IDH*-wildtype glioblastoma and astrocytoma *IDH*-mutant grade 4 at imaging and transcriptomic levels. *NMR in Biomedicine*. 2023;36(11):e5004. doi:10.1002/nbm.5004